Effect of dislocations on minority carrier diffusion length in practical silicon solar cells

Thomas Kieliba,[a] Stephan Riepe, and Wilhelm Warta
Fraunhofer Institute for Solar Energy Systems, Heidenhofstrasse 2, 79110 Freiburg, Germany

(Received 29 March 2006; accepted 1 June 2006; published online 22 September 2006)

In 1998, Donolato presented an analytical model describing the effect of dislocation density on minority carrier effective diffusion length [J. Appl. Phys. **84**, 2656 (1998)]. While this analysis was derived for a "semi-infinite" specimen, our objective is the appropriate description of thin devices, such as wafer or thin-film based crystalline Si solar cells with back surface field or passivating layer on the rear side. Therefore, Donolato's model is extended for specimen of finite thickness and finite recombination velocity at the back surface. Since the associated boundary value problem does not allow a straightforward analytical solution, we derive an approximate expression, which is validated by numerical simulations. In the original work, Donolato uses a special definition of an "effective diffusion length." This definition is different from the quantity usually referred to as effective diffusion length when analyzing quantum efficiency data. Furthermore, Donolato's definition does not refer to the typical operation conditions of a solar cell. We therefore modify Donolato's model for the effect of dislocations consistently using the quantum efficiency effective diffusion length. Finally, our model is applied to the determination of dislocation recombination strength in thin-film solar cells with back surface field from effective diffusion length maps. © *2006 American Institute of Physics*. [DOI: 10.1063/1.2338126]

I. INTRODUCTION

Different models have been proposed to describe the effect of dislocations on minority carrier effective lifetime or diffusion length.[1–3] The model developed by Donolato[4,5] starts from a geometric description that is much closer to the physical reality than most of the models developed before. The predicted dependence of effective diffusion length on dislocation density matches well to experimental data and has been used to evaluate dislocation recombination strength values on Si solar cells.[6–10] Starting from the same geometrical arrangement as used by Donolato, we have correlated spatially resolved effective lifetimes measured under steady state conditions with dislocation density, yielding compatible recombination strength values for unprocessed multicrystalline Si wafers.[11]

Donolato analyzed the effect of dislocations from the viewpoint of charge collection at a junction of a semi-infinite dislocation-containing specimen.[4] For actual devices, such as *p-n* junction crystalline Si solar cells, this model is an adequate approximation as long as the bulk diffusion length is much smaller than the base thickness. However, in many of today's solar cells, the bulk diffusion length exceeds the cell thickness, and this is also true for well-designed *p-n* junction thin-film solar cells. Although Donolato has extended his analysis for the case of finite thickness and infinite rear surface recombination velocity, again, these conditions do not fit to our objectives since standard industrial as well as thin-film solar cells incorporate structures to decrease recombination at the rear side.

Therefore, a major task of this work is to extend Donolato's model for devices with finite thickness and finite rear surface recombination velocity. Another aspect addressed in this work is the transformation of the model to a more generally used definition of effective diffusion length, which is especially suitable for experimental comparison to quantum efficiency measurements.

II. ANALYTICAL MODEL

A. Donolato's model for the effect of dislocations on effective diffusion length

Boundary value problem. All of the following analysis is based on carrier collection at the interface plane of a charge neutral semiconductor, as sketched in Fig. 1(a). This interface may be a *p-n* junction, located at the origin of the depth coordinate ($z=0$). Furthermore, we assume ideal collection properties at the interface. In terms of charge collection probability φ these assumptions manifest in the boundary condition

$$\varphi(0) = 1. \tag{1}$$

If the specimen is described as a half space that extends infinitely in the positive z direction (referred to as "semi-infinite" case) the boundary condition

$$\lim_{z\to\infty} \varphi(z) = 0 \tag{2}$$

applies.

The one-dimensional inhomogeneous carrier transport equation corresponds to a homogeneous equation for the collection probability, as shown by the reciprocity theorem of charge collection.[12–17] Therefore the equation to be solved reads

[a]Author to whom correspondence should be addressed; present address: ErSol Solar Energy AG, Wilhelm-Wolff-Str. 23, 99099 Erfurt, Germany; FAX: +49 361 2195-205; electronic mail: thomas.kieliba@ersol.de

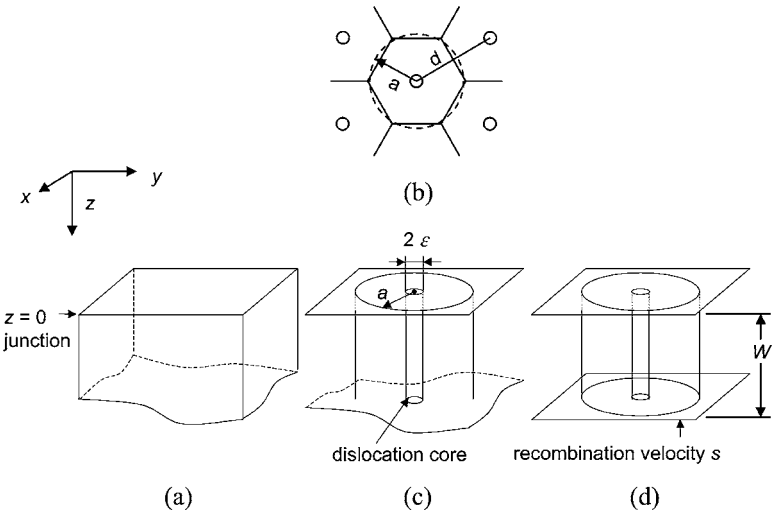

FIG. 1. Schematic device structures: (a) Semi-infinite specimen with homogeneous material properties. (b) Top view on dislocation array and approximation of the hexagonal unit cell by a cylinder. (c) Semi-infinite specimen with dislocation core and unit cell. (d) Dislocated specimen of finite thickness and finite surface recombination velocity at the rear.

$$\left(\frac{d^2}{dz^2} - \frac{1}{L^2}\right)\varphi(z) = 0, \tag{3}$$

where L denotes the bulk diffusion length. The solution of the boundary problem is given by the simple exponentially decaying function

$$\varphi(z) = \exp(-z/L). \tag{4}$$

The geometric arrangement for Donolato's model of a dislocation-containing specimen is a modification of the arrangement discussed above [Fig. 1(a)]. Again, the basis is a neutral semiconductor half space ($z>0$) where the surface plane ($z=0$) coincides with the edge of the p-n junction. Dislocations are assumed as a hexagonal array of straight dislocation lines perpendicular to the surface with spacing d [Fig. 1(b)]. Because of the periodicity of the arrangement, the carrier transport problem can be restricted to one unit cell. Approximating the hexagonal unit cell by a cylindrical cell with radius a, the problem can be treated in cylindrical coordinates [Fig. 1(c)].

Dislocation density ρ_d and radius a are then related by

$$\rho_d = \frac{1}{\pi a^2}. \tag{5}$$

The dislocation is described as a recombination line, characterized by a line recombination velocity γ_d, which is also called *recombination strength*.[18] The model assumes that γ_d is constant and therefore it is strictly valid for low injection conditions only. Dividing γ_d by the diffusion constant D, we obtain the dimensionless parameter *normalized recombination strength*

$$\Gamma_d = \frac{\gamma_d}{D}. \tag{6}$$

Treating the boundary value problem in cylindrical coordinates, condition (1) at the junction plane ($z=0$) becomes

$$\varphi(r,0) = 1, \tag{7}$$

while condition (2) for the limit $z\to\infty$ reads

$$\lim_{z\to\infty} \varphi(r,z) = 0. \tag{8}$$

For symmetry reasons, the radial gradient of φ must vanish at the cylinder's surface ($r=a$), yielding the boundary condition

$$\left.\frac{\partial\varphi}{\partial r}\right|_{r=a} = 0. \tag{9}$$

Finally, we have the boundary condition at the recombination line[4]

$$\lim_{r\to 0}\left(2\pi r\frac{\partial\varphi}{\partial r}\right) = \Gamma_d\varphi(0,z). \tag{10}$$

Without the dislocation line, the boundary value problem is the same as discussed before [Eqs. (1)–(3)] with solution $\exp(-z/L)$. To solve the transport equation [Eq. (3)] for the dislocated specimen, Donolato therefore uses the ansatz

$$\varphi(r,z) = \exp(-z/L_0) - u(r,z), \tag{11}$$

where L_0 denotes the bulk diffusion length in the dislocation-free specimen. Employing the Fourier sine transform of u, the transport equation (in cylindrical coordinates) can be transformed into an ordinary differential equation for which the analytical solution is known.[19] In order to circumvent a singularity of the Fourier sine transform of u, Donolato performs an averaging over a small circle with radius ε around $r=0$. From a physical point of view, this approximation can be interpreted as attributing a finite cross section ε to the dislocation line [see Fig. 1(c)].

If minority carriers are generated with homogeneous rate G ($\mathrm{m^{-3}\,s^{-1}}$) within a (unit) cell of volume V_c, the current density collected at the junction is

$$J_{\mathrm{sc}} = \frac{qG}{A}\int_{V_c}\varphi(\mathbf{r})dV, \tag{12}$$

where A denotes the junction area.

For the semi-infinite reference specimen with homogeneous diffusion length L [Fig. 1(a)], the charge collection probability is given by Eq. (4), and Eq. (12) yields

$$J_{\mathrm{sc,ref}} = qLG. \tag{13}$$

Donolato now defines the effective diffusion length $L_{\mathrm{eff},D}$ as the value of L for which the current density of the semi-infinite reference specimen $J_{\mathrm{sc,ref}}$ is equal to that of the arbitrary specimen J_{sc} given by Eq. (12). Therefore

$$L_{\mathrm{eff},D} = \frac{1}{A}\int_{V_c} \varphi(\mathbf{r})dV. \tag{14}$$

By solving the transport equation with the boundary conditions above, the effective diffusion length in the dislocated specimen can be expressed by[4,5]

$$L_{\mathrm{eff},D} = L_0 - \frac{2}{\pi}\rho_d\Gamma_d\int_0^\infty \frac{1}{\mu^4}\frac{dk}{1+(\Gamma_d/\pi)H(\mu\varepsilon,\mu a)}, \tag{15}$$

where

$$H(\mu\varepsilon,\mu a) = \frac{1-\mu\varepsilon K_1(\mu\varepsilon)}{\mu^2\varepsilon^2} + \frac{I_1(\mu\varepsilon)K_1(\mu a)}{\mu\varepsilon I_1(\mu a)}, \tag{16}$$

with modified Bessel functions of order one I_1 and K_1, and

$$\mu = \sqrt{k^2 + \frac{1}{L_0^2}}. \tag{17}$$

B. Modification for effective diffusion length based on IQE measurements

In the model above, Donolato's definition of effective diffusion length has been used. From practical and physical points of view, there are some disadvantages in this definition: (i) $L_{\mathrm{eff},D}$ is not compatible with standard measurement methods that rely on the slope of IQE^{-1} vs α^{-1} curves, (ii) $L_{\mathrm{eff},D}$ differs from the effective diffusion length L_{eff,J_0} (see below) that determines the solar cell's open circuit voltage, and (iii) most importantly, homogeneous generation does not correspond to the typical operation conditions of a solar cell. Photons with near band-gap energy contribute to a very small part of total irradiated energy only. Therefore, we modified Donolato's analysis to be compatible with the quantum efficiency effective diffusion length.

Collection effective diffusion length. In practical solar cell devices, the case of homogenous generation is found for wavelengths with energy near the band gap and it yields a second linear regime of the IQE^{-1} vs α^{-1} curve. The inverse slope at this region has been defined as *collection effective diffusion length*[20] by

$$\frac{1}{L_{\mathrm{eff},c}} = \left.\frac{d\mathrm{IQE}^{-1}}{d\alpha^{-1}}\right|_{\alpha^{-1}=\infty}, \tag{18}$$

where the index $(\alpha^{-1}=\infty)$ indicates the evaluation at large absorption length. The internal quantum efficiency (IQE) is related to the charge collection probability φ by

$$\mathrm{IQE}(\lambda) = \int_0^W \frac{G_\lambda(z)}{E_{p,\lambda}(0)}\varphi(z)dz, \tag{19}$$

where W is the device thickness and G_λ $(\mathrm{m^{-3}\,nm^{-1}\,s^{-1}})$ is the spectral generation rate, normalized by the net incident spectral photon flux $E_{p,\lambda}(0)$ $(\mathrm{m^{-2}\,nm^{-1}\,s^{-1}})$ on the illuminated side of the device. $E_{p,\lambda}(0)$ is obtained by subtracting the components due to reflection and escape from the total incident flux.

The collection efficiency η_c is given by

$$\eta_c(\lambda) = \int_0^W g(\lambda,z)\varphi(z)dz, \tag{20}$$

where g $(\mathrm{m^{-1}})$ is the normalized generation rate defined through the condition

$$\int_0^W g(\lambda,z)dz \equiv 1. \tag{21}$$

IQE and η_c are connected by $\mathrm{IQE}=f_{\mathrm{abs}}\,\eta_c/(1-R)$, where f_{abs} is the fraction of photons absorbed and R is the sum of hemispherical reflection and escape at the front surface.[21] IQE and η_c are identical if $f_{\mathrm{abs}}=1-R$. This is the case when no light is transmitted at the rear side of the device and no parasitic absorption occurs (such as absorption in an antireflection coating).

Basore has developed an analytical model that allows one to assess the internal optical properties of a solar cell from the quantity $L_{\mathrm{eff},c}$.[21] Using a linear approximation, $L_{\mathrm{eff},c}$ is connected to the collection efficiency for near band-gap wavelength $\eta_{c,\infty}$ by

$$L_{\mathrm{eff},c} = f_{\mathrm{opt}} W \eta_{c,\infty}, \tag{22}$$

where f_{opt} is a function that solely depends on the internal optical properties of the solar cell.

We can easily derive the connection between the collection effective diffusion length $L_{\mathrm{eff},c}$ and the effective diffusion length as defined by Donolato $L_{\mathrm{eff},D}$. For spatially homogeneous generation, the normalized generation rate g given by Eq. (21) must be equal to $1/W$. Insertion of $g=1/W$ into Eq. (20), use of Eq. (31) (see below), and comparison with Eq. (14) yield

$$\eta_{c,\infty} = \frac{1}{W}L_{\mathrm{eff},D}. \tag{23}$$

Referring to Eq. (22), we find that the collection efficiency effective diffusion length $L_{\mathrm{eff},c}$ and Donolato's effective diffusion length $L_{\mathrm{eff},D}$ are related by

$$L_{\mathrm{eff},c} = f_{\mathrm{opt}} L_{\mathrm{eff},D} \tag{24}$$

and differ only by the function f_{opt}.

Quantum efficiency effective diffusion length. A standard measurement tool for the investigation of solar cells is the measurement of the external quantum efficiency (EQE). By incorporating reflection measurement data, the IQE can be extracted.

For the semi-infinite solar cell, the spectral generation rate is given by

$$G_\lambda(z) = E_{p,\lambda}(0)\alpha(\lambda)\exp[-\alpha(\lambda)z]. \tag{25}$$

It is easily shown that insertion of Eq. (25) into Eq. (19) and performing the integration for $W\to\infty$ yield a linear relationship between the inverse internal quantum efficiency (IQE^{-1}) (which in this case is equal to the inverse collection efficiency η_c^{-1}) and the inverse absorption length α^{-1}

TABLE I. Comparison of different definitions of effective diffusion length. They all relate a particular quantity for an arbitrary specimen to the equivalent quantity of a semi-infinite reference specimen with homogeneous diffusion L_{eff} and collection probability $\varphi(z)=\exp(-z/L_{\mathrm{eff}})$.

	Quantum efficiency effective diffusion length	Current-voltage effective diffusion length	Donolato's effective diffusion length	Collection efficiency effective diffusion length
Symbol	$L_{\mathrm{eff,IQE}}$	L_{eff,J_0}	$L_{\mathrm{eff},D}$	$L_{\mathrm{eff},c}$
Quantity compared with reference	$\left.\frac{d\eta_c^{-1}}{d\alpha^{-1}}\right\vert_{\alpha^{-1}=0}$	J_0	I_{sc} for homogeneous generation (without int. refl.)	I_{sc} for homogeneous generation (incl. int. refl.)
Relation to collection efficiency φ	$\frac{1}{L_{\mathrm{eff,IQE}}} \propto \left.\frac{\partial\varphi}{\partial z}\right\vert_{z=0}$	$\frac{1}{L_{\mathrm{eff},J_0}} \propto \left.\frac{\partial\varphi}{\partial z}\right\vert_{z=0}$	$L_{\mathrm{eff},D} \propto \int_{V_c}\varphi(\mathbf{r})dV$	$L_{\mathrm{eff},c} \propto f_{\mathrm{opt}}\int_{V_c}\varphi(\mathbf{r})dV$
Connection	$L_{\mathrm{eff,IQE}} \equiv L_{\mathrm{eff},J0}$		$L_{\mathrm{eff},c} \equiv f_{\mathrm{opt}} L_{\mathrm{eff},D}$	

$$\frac{1}{\mathrm{IQE}(\lambda)} = \frac{1}{\alpha(\lambda)L} + 1. \tag{26}$$

Relation (26) is the starting point for diffusion length extraction from quantum efficiency data.[22] However, real devices do not extend infinitely and often material properties are not homogeneous, as is generally the case for multicrystalline solar cells. Still, in many cases the projection of the three-dimensional charge collection probability $\varphi(\mathbf{r})$ on the z coordinate can be well approximated by the one-dimensional function

$$\varphi(z) = \exp(-z/L_{\mathrm{eff}}). \tag{27}$$

A prerequisite for this approximation to be valid is a bulk diffusion length L smaller than the device thickness W. If Eq. (27) describes the actual collection efficiency function well, then Eq. (26) holds with L replaced by L_{eff}. With the constraint $L \ll W$, Dugas and Qualid have defined an effective diffusion length by the slope $1/L_{\mathrm{eff}}$ of a linear fit to the IQE^{-1} vs α^{-1} graph in the regime $W_e \ll \alpha^{-1} \ll W$, where W_e is the emitter thickness.[23]

In many of today's crystalline Si solar cells, the bulk diffusion length exceeds the cell thickness. In this case, the linear relationship by Eq. (26) does not hold anymore and the IQE^{-1} vs α^{-1} graph is curved.[24,25]

A general definition of effective diffusion length therefore has to use a fixed absorption length at which the slope of the IQE^{-1} vs α^{-1} curve is evaluated. This is taken into account in the following definition of *quantum efficiency effective diffusion length* $L_{\mathrm{eff,IQE}}$:[20]

$$\frac{1}{L_{\mathrm{eff,IQE}}} = \left.\frac{d\eta_c^{-1}}{d\alpha^{-1}}\right\vert_{\alpha^{-1}=0} \cong \left.\frac{d\mathrm{IQE}^{-1}}{d\alpha^{-1}}\right\vert_{\alpha^{-1}=0}. \tag{28}$$

While the evaluation at $\alpha^{-1}=0$ is advantageous from theoretical considerations—as shown below—a drawback from a practical point of view is that for real solar cells the slope of the IQE^{-1} vs α^{-1} curve at $\alpha^{-1}=0$ is dominated by the emitter of thickness W_e. The computation of the base effective diffusion length $L_{\mathrm{eff,IQE}}$ as defined by Eq. (28) therefore requires an extrapolating fit to the IQE^{-1} vs α^{-1} curve from the region $W_e < \alpha^{-1} < W$ to the point $\alpha^{-1}=0$.[24,25]

Relation to effective diffusion length extracted from saturation current. For considerations later on in this work, we need to look into another definition of L_{eff}, which is based on the saturation current density J_0. For a semi-infinite device with homogeneous electronic properties as sketched in Fig. 1(a), saturation current density $J_{0,\infty}$ and bulk diffusion length L are connected by

$$J_{0,\infty} = \frac{qD_n n_0}{L}, \tag{29}$$

where n_0 is the minority carrier equilibrium density and D_n is their diffusion constant. This formula is usually derived by studying the decay of the minority carrier concentration in neutral regions for injection at the junction interface.[26] Starting from the charge collection probability φ, the minority carrier density at high reverse bias in the dark is $n_0(1\text{-}\varphi)$,[27] and for an arbitrary specimen, the saturation current density is given by

$$J_0 = qn_0 D_n \left.\frac{d\varphi(z)}{dz}\right\vert_{z=0}, \tag{30}$$

where the projection $\varphi(z)$ of the three-dimensional collection probability function $\varphi(x,y,z)$ is obtained by integration over the (unit) cell area A of the junction plane

$$\varphi(z) = \frac{1}{A}\int_y\int_x \varphi(x,y,z)dxdy. \tag{31}$$

A *current-voltage effective diffusion length* L_{eff,J_0} (Ref. 28) can be defined as the value of L for which the saturation current density of the semi-infinite reference specimen $J_{0,\infty}$ given by Eq. (29) is equal to that of the arbitrary specimen J_0 [Eq. (30)]. Therefore

$$L_{\mathrm{eff},J_0} = \frac{qD_n n_0}{J_0}. \tag{32}$$

Table I summarizes the main aspects of the different

definitions of effective diffusion length. The way quantum efficiency effective diffusion length $L_{\mathrm{eff,IQE}}$ and current-voltage diffusion length L_{eff,J_0} has been introduced, they must be identical by definition.[21] On the base of the charge collection reciprocity theorem, Brendel and Rau have proven that the equality $L_{\mathrm{eff,IQE}} \equiv L_{\mathrm{eff},J_0}$ also holds for material with inhomogeneous diffusion constant and carrier lifetime.[29] If potential fluctuations are taken into account, this relation still holds locally, while for the global electronic properties $L_{\mathrm{eff,IQE}} > L_{\mathrm{eff},J_0}$.

Effect of dislocations using the quantum efficiency effective diffusion length. In order to modify Donolato's model for use with the quantum efficiency effective diffusion length $L_{\mathrm{eff,IQE}}$, we can make use of the identity $L_{\mathrm{eff,IQE}} \equiv L_{\mathrm{eff},J_0}$. The right hand side is evaluated by definition (32) and Eq. (30). Using the relationship $A = \pi a^2 = 1/\rho_d$ for the junction area of the unit cell, the average saturation current density is given by

$$\bar{J}_{0,B} = \frac{I_{0,B}}{A} = \rho_d I_{0,B} = -\rho_d q D_n n_0 \int_0^a \left.\frac{\partial \varphi}{\partial z}\right|_{z=0} 2\pi r dr. \quad (33)$$

The charge collection probability, which has to be inserted into this equation, is[5]

$$\varphi(r,z) = \exp(-z/L_0) + \frac{\Gamma_d}{\pi^2}\int_0^\infty \frac{k}{\mu^2}\frac{K_0(\mu r) + I_0(\mu r)K_1(\mu a)/I_1(\mu a)}{1 + (\Gamma_d/\pi)H(\mu\varepsilon,\mu a)}dk. \quad (34)$$

The differentiation with respect to z and the integration over the volume (i.e., r and z) can be performed analytically. However, this is not possible for the wave vector k and the final expression then is

$$\frac{1}{L_{\mathrm{eff,IQE}}} = \frac{1}{L_0} + \frac{2}{\pi}\rho_d\Gamma_d\int_0^\infty \frac{k^2}{\mu^4}\frac{dk}{1 + (\Gamma_d/\pi)H(\mu\varepsilon,\mu a)}. \quad (35)$$

Comparing this expression with the one for $L_{\mathrm{eff},D}$ [Eq. (15)], we note the following difference in structure: While in Eq. (15) the effective diffusion length $L_{\mathrm{eff},D}$ is obtained by subtracting a dislocation term from the diffusion length in the dislocation-free sample L_0, in Eq. (35) the inverse effective diffusion length $L_{\mathrm{eff,IQE}}^{-1}$ is the sum of the inverse diffusion length L_0^{-1} and the dislocation term. This finding becomes clear when we recall the definition of current-voltage effective diffusion length [Eq. (32)]. The effective diffusion length $L_{\mathrm{eff,IQE}}$ is proportional to the inverse of the total recombination current, which equals the recombination current in the device without dislocations, plus the dislocation induced recombination current. This behavior is similar to a situation analyzed by Sinton, who discussed the averaging of effective lifetime in a multicrystalline wafer with highly conductive emitter and grains exhibiting different bulk lifetimes.[30]

C. Approximation for sample of infinite thickness

In order to fit the functions $L_{\mathrm{eff},D}(\rho_d)$ or $L_{\mathrm{eff,IQE}}(\rho_d)$ to experimental data the forms given by Eqs. (15) and (35) respectively, are not very convenient. The numerical evaluation of the integral is time consuming since at each interpolation node several Bessel functions have to be evaluated. For $L_{\mathrm{eff},D}$ given by Eq. (15) Donolato has derived a closed form approximation[4]

$$L_{\mathrm{eff}}(\rho_d) \cong \left\{\frac{1}{L_0^2} + \frac{\rho_d\Gamma_d}{1 + (\Gamma_d/2\pi)[-\ln(\varepsilon\sqrt{\pi\rho_d}) - C + 1/2]}\right\}^{-1/2}, \quad (36)$$

where C is Euler's gamma constant, with numerical value $\approx 0.577\,216$.

It can be shown that exactly the same expression is obtained for $L_{\mathrm{eff,IQE}}$ by Eq. (35) when using the identical approximations that are involved in the derivation of Eq. (36) from Eq. (15). However, for $L_{\mathrm{eff,IQE}}$ the approximations used are strictly valid for very high dislocation density only ($\rho_d > 10^7\ \mathrm{cm}^{-2}$) and Eq. (36) does not approximate $L_{\mathrm{eff,IQE}}(\rho_d)$ quite as well as it does $L_{\mathrm{eff},D}(\rho_d)$.

For example, in Fig. 2 the modeled dependence of L_{eff} on ρ_d is plotted using typical device data. The function $L_{\mathrm{eff}}(\rho_d)$ was calculated (i) based on Donolato's definition of effective diffusion length [Eq. (15)], (ii) the quantum efficiency effective diffusion length [Eq. (35)], and (iii) the approximate form given by Eq. (36). The only slight difference between the three curves is visible in the region of very high dislocation density. In this region, $L_{\mathrm{eff,IQE}}(\rho_d)$ differs marginally from $L_{\mathrm{eff},D}(\rho_d)$ and the approximate form $L_{\mathrm{eff}}(\rho_d)$. Two reasons might be responsible. Firstly, it is clear from the approximations involved that $L_{\mathrm{eff}}(\rho_d)$ does not approximate $L_{\mathrm{eff,IQE}}(\rho_d)$ as well as it does $L_{\mathrm{eff},D}(\rho_d)$. Secondly, the difference may also be caused by the numerical integration of the "exact" formulas.

By definition, $L_{\mathrm{eff},D}(\rho_d)$ and $L_{\mathrm{eff,IQE}}(\rho_d)$ are identical for the special charge collection probability function $\varphi_{\mathrm{ref}}(z) = \exp(-z/L_{\mathrm{eff}})$. Therefore, if for an arbitrary three-dimensional charge collection probability function $\varphi(\mathbf{r})$,

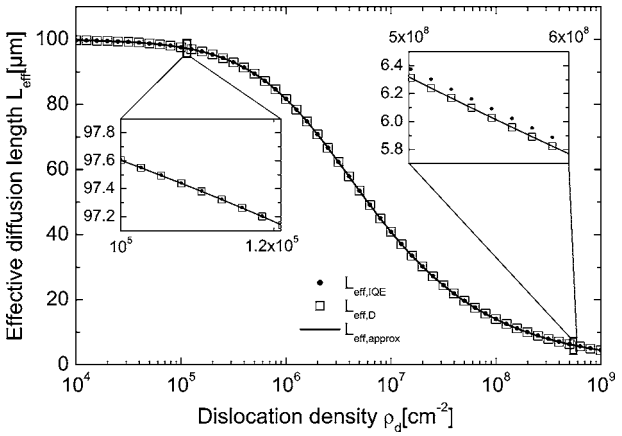

FIG. 2. Dependence of effective diffusion length on dislocation density for the semi-infinite specimen. Compared are the exact functions $L_{\mathrm{eff},D}(\rho_d)$ by Eq. (15), $L_{\mathrm{eff,IQE}}(\rho_d)$ by Eq. (35), and the approximate form by Eq. (36). For numerical evaluation of the exact expressions the upper integration limit was set to $1000/L_0$. (Fixed parameters: $\varepsilon = 0.01\ \mu$m, $L_0 = 100\ \mu$m, and $\Gamma_d = 0.005$.)

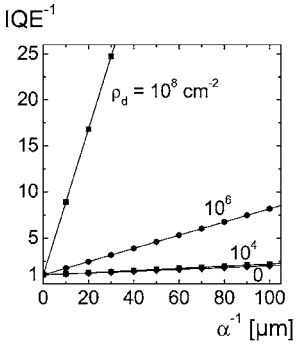

(a)

ρ_d [cm^{-2}]	Fit A 0.01 – 0.05 μm L_{eff} [μm]	$L_{eff,IQE}$ [μm]	Fit B 10 – 100 μm L_{eff} [μm]	$L_{eff,D}$ [μm]
0	100.0	100.0	100.0	100.0
10^4	83.23	83.22	83.62	83.63
10^6	13.74	13.72	13.89	13.89
10^8	1.254	1.253	1.265	1.265

Fixed parameters: $L_0 = 100$ μm, $\Gamma_d = 1$, $\varepsilon = 0.01$ μm

(b)

FIG. 3. (a) Plots of IQE^{-1} vs α^{-1} using Donolato's model for the effect of dislocations. (b) Comparison of numerical data for L_{eff} obtained from linear fits to the plots in part (a) (fit A with fitting range $\alpha^{-1} = 0.01 - 0.05$ μm; fit B with fitting range $\alpha^{-1} = 10 - 100$ μm), and calculation of $L_{eff,D}$ and $L_{eff,IQE}$ by Eqs. (15) and (35), respectively. The fits were not forced to go through (0,1).

$L_{eff,D}(\rho_d)$, and $L_{eff,IQE}(\rho_d)$ yield similar values, it can be concluded that the dislocated semi-infinite specimen can be quite well described by the one-dimensional charge collection probability function $\varphi(z) = \exp(-z/L_{eff})$ [Eq. (27)].

The finding above is supported by the data shown in Fig. 3, in which L_{eff} values from linear fits to the IQE^{-1} vs α^{-1} curve are compared to results by Eqs. (15) and (35). On one hand, the function IQE$^{-1}(\alpha^{-1})$ was evaluated at discrete absorption length values α_i^{-1} using Eqs. (19), (25), and (34). Then, L_{eff} was determined from a fit to the data points IQE$^{-1}(\alpha_i^{-1})$. In case A, L_{eff} was evaluated based on data points at $\alpha_1^{-1} = 0.01$ μm, $\alpha_2^{-1} = 0.02$ μm, …, $\alpha_5^{-1} = 0.05$ μm. In case B, L_{eff} was evaluated based on data points at $\alpha_1^{-1} = 10$ μm, $\alpha_2^{-1} = 20$ μm…, $\alpha_{10}^{-1} = 100$ μm. On the other hand, $L_{eff,D}(\rho_d)$ and $L_{eff,IQE}(\rho_d)$ were computed by Eqs. (15) and (35), respectively.

Although the four L_{eff} values for each ρ_d are quite similar, it is instructive to take a closer look at the small differences after the decimal point. For case A the fit results are practically identical to the values of $L_{eff,IQE}$, while for case B the fit results are more close to the values of $L_{eff,D}$. This finding makes sense when recalling that $L_{eff,IQE}$ is defined by the slope of the function IQE$^{-1}(\alpha^{-1})$ at $\alpha^{-1} = 0$ while $L_{eff,D}$ depends on the slope of IQE$^{-1}(\alpha^{-1})$ for homogeneous generation (usually corresponding to large α^{-1}). Note that for the ideal semi-infinite specimen there is complete light absorption and no optical properties of the rear side have to be considered. Therefore, in this case $\eta_c = \text{IQE}$ and $L_{eff,c} \equiv L_{eff,D}$. A rough dimension criterion to divide between the two regimes is the diameter of the unit cell—e.g., 0.56 μm for $\rho_d = 10^8$ cm^{-2} and 56 μm for $\rho_d = 10^4$ cm^{-2}, respectively. If we assume that the dislocation line only enhances recombination in a low volume fraction, we can conclude that the radial variation in collection probability is small compared to the one in the z direction. This is true even though the data in Fig. 3 were calculated using a very high value for the recombination strength Γ_d. Typical experimentally determined values are much lower (see Table V). The argument discussed above explains why both evaluation methods lead to similar results and the collection probability can well be approximated by $\varphi(z) = \exp(-z/L_{eff})$.

For practical purposes, we can conclude that in the case of the semi-infinite semiconductor it does not matter whether the quantum efficiency definition or Donolato's definition of effective diffusion length is used to calculate the function $L_{eff}(\rho_d)$.

D. Model for a specimen of finite thickness

For a specimen of finite thickness and with finite surface recombination at the rear [Fig. 1(c)], boundary condition (8) has to be replaced by

$$\left.\frac{d\varphi(r,z)}{dz}\right|_{z=W} = -s\varphi(r,W), \tag{37}$$

where s is the reduced surface recombination velocity ($s = S/D$). With this condition, an approach equivalent to Eq. (11), which enables the transformation of the partial differential equation into an ordinary differential equation, is not possible. The solution in the z direction is no longer independent from the radial solution. To evaluate the left hand side of Eq. (37), the knowledge of the radial function $\varphi(r,W)$ would be necessary.

Instead of finding an exact solution to the boundary value problem, we show that a good approximation is possible if we split up the problem into two steps: (i) calculation of the collection probability for the case of a dislocated semi-infinite specimen, yielding a one-dimensional projection of the charge collection probability function on the z axis $\varphi(z)$, and (ii) "cutting off" the specimen at finite thickness by applying the appropriate boundary condition.

A hint for the validity of the approximation involved in step (i) was given in the section before. The similarity of $L_{eff,D}(\rho_d)$ and $L_{eff,IQE}(\rho_d)$, as well as the linearity of the IQE^{-1} vs α^{-1} curves (Fig. 3), indicates that the charge collection probability $\varphi(r,z)$ in the dislocated semi-infinite specimen is well described by the one-dimensional exponential decay $\varphi(z) = \exp(z/L_{eff})$.

Furthermore, physical arguments can be given for our "two-step approach." Typical dislocation densities in multicrystalline Si range from 10^4 to 10^8 cm^{-2}, corresponding to average dislocation distances d ranging from 100 to 1 μm. For very high recombination strength ($\Gamma_d = 1$), the effective diffusion length is in the same range as the average dislocation distance, as can be taken from the numbers tabulated in Fig. 3(b). However, typical Γ_d values are much lower ranging between 0.1 and 0.001. Therefore, the effective diffusion length exceeds the average dislocation distance. For example, $L_0 = 100$ μm, $\Gamma_d = 0.01$, and $\rho_d = 10^6$ cm^{-2} yield $L_{eff} = 71$ μm, while the corresponding dislocation distance is 11 μm. This finding is reasonable since the small cross section of a dislocation should affect carrier transport much less than a recombination-enhancing surface. From the viewpoint

TABLE II. Dependence of effective diffusion length $L_{\text{eff},D}$ on dislocation density for a semiconductor of finite thickness and infinite surface recombination velocity at the back. For model A the values were calculated by the exact formula [Eq. (39)] while for model B the approximating "two-step approach" was used (for details see text). (Fixed parameters: $W=30$ μm, $\varepsilon=0.01$ μm, and $L_0=100$ μm.).

		$L_{\text{eff},D}$ (μm)	
Γ_d	ρ_d (cm^{-2})	Model A	Model B
0.001	10^4	14.8884	14.8884
	10^8	13.8744	13.8744
	10^{12}	0.3162	0.3162
1	10^4	14.8(380)	14.8(412)
	10^8	1.2649	1.2649
	10^{12}	0.01(02)	0.01(13)

of the device, the above consideration justifies to model the dislocated material with homogeneous recombination properties.

Practically our approach is performed by (i) calculating the bulk effective diffusion length $L_{\text{eff},b}$ for the semi-infinite specimen containing dislocations by Eq. (15), (35), or (36) and (ii) inserting $L_{\text{eff},b}$ and the back surface recombination velocity s into

$$\varphi(z)=\frac{\cosh[(W-z)/L_{\text{eff},b}]+L_{\text{eff},b}s\,\sinh[(W-z)/L_{\text{eff},b}]}{\cosh(W/L_{\text{eff},b})+Ls\,\sinh(W/L_{\text{eff},b})}. \tag{38}$$

[The above equation is the general solution to problem (3) with boundary conditions (1) and $d\varphi/dz=-s\varphi$ at $z=W$.] Finally, $\varphi(z)$ is used to obtain $L_{\text{eff},D}$ by Eq. (14) or $L_{\text{eff,IQE}}=L_{\text{eff},J_0}$ by Eqs. (30) and (32). In our model, the back surface recombination velocity is assumed independent from the number and recombination strength of dislocations. For high dislocation densities, this assumption may not be valid.

We test the two-step approach for a specimen of finite thickness and infinite surface recombination velocity. For this special case, an analytical solution exists[4]

$$L_{\text{eff},D}=L_0\tanh\left(\frac{W}{2L_0}\right)-\frac{4}{W}\rho_d\Gamma_d\sum_{n=1}^{\infty}\frac{1}{\mu_n^4[1+(\Gamma_d/\pi)H(\mu_n\varepsilon,\mu_n a)]},\quad n\ \text{odd}, \tag{39}$$

where $\mu_n=(k_n^2+1/L_0^2)^{1/2}$. Table II presents computed data for parameters covering a broad range of dislocation density and recombination strength values. For numerical evaluation of Eq. (39) (model A) the sum was computed for 1000 terms, while for Eq. (15) (model B) the upper integration limit was set to $10\,000/L_0$. It was only in the case of an untypically high recombination strength $\Gamma_d=1$ that marginal differences were found.

While for the semi-infinite specimen the functions $L_{\text{eff},D}(\rho_d)$ and $L_{\text{eff,IQE}}(\rho_d)$) practically yield the same result (Fig. 2), the situation is completely different for the case of finite thickness. Figure 4 shows that $L_{\text{eff},D}(\rho_d)$ and $L_{\text{eff,IQE}}(\rho_d)$ approach different limits for $\rho_d\to 0$. Table III summarizes these limits for $\rho_d\to 0$, considering several extreme combinations of surface recombination velocity s and diffusion length L_0.

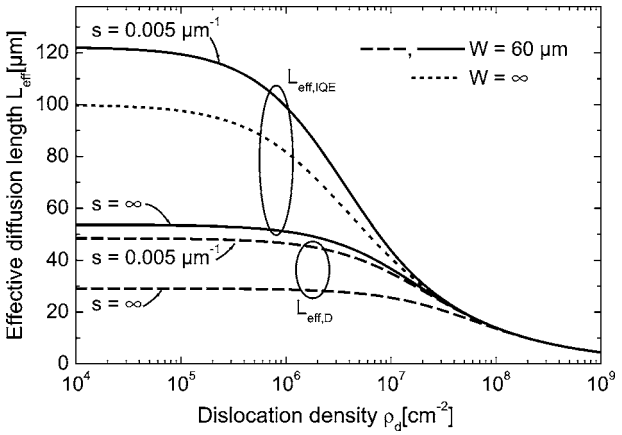

FIG. 4. Dependence of effective diffusion length L_{eff} on dislocation density ρ_d for a specimen of finite thickness W. The functions based on Donolato's definition of effective diffusion length $L_{\text{eff},D}$ (dashed lines) are different from those based on the quantum efficiency definition of effective diffusion length $L_{\text{eff,IQE}}$ (solid lines). For comparison, the dependence is shown for the semi-infinite specimen (dotted line). In this case $L_{\text{eff},D}$ and $L_{\text{eff,IQE}}$ are (approximately) equal. (Fixed parameters: $\varepsilon=0.01$ μm, $L_0=100$ μm, and $\Gamma_d=0.005$.)

III. EXPERIMENTAL RESULTS

A. Sample preparation

The model developed above was applied to the analysis of crystalline Si thin-film solar cells with silicon-on-insulator (SOI) structure. Standard ~300 μm thick multicrystalline Si wafers served as substrate. These were coated with a 2 μm thick plasma-enhanced chemical vapor deposition (PECVD) intermediate oxide before deposition of 5 μm highly doped (3×10^{18} cm^{-3}) Si by atmospheric pressure chemical vapor deposition (APCVD). Subsequently, the thin Si film was recrystallized by zone-melting recrystallization (ZMR), enlarging grain size to typically several millimeters in width and several centimeters in length. During the ZMR process, the Si film was coated with a 2 μm thick PECVD capping oxide to prevent agglomeration of molten Si. Afterwards, the oxide was removed in HF and the recrystallized Si film served as

TABLE III. Limits of the functions $L_{\text{eff},D}(\rho_d)$ and $L_{\text{eff,IQE}}(\rho_d)$ in the case $\rho_d\to 0$ for a specimen of thickness W.

s	L_0	$L_{\text{eff},D}$	$L_{\text{eff,IQE}}$
∞	∞	$\frac{W}{2}$	W
Finite	∞	$\frac{W(Ws+2)}{2(Ws+1)}$	$W+\frac{1}{s}$
0	Finite	$L_0\tanh\left(\frac{W}{2L_0}\right)$	$L_0\coth\left(\frac{W}{L_0}\right)$
0	∞	W	∞

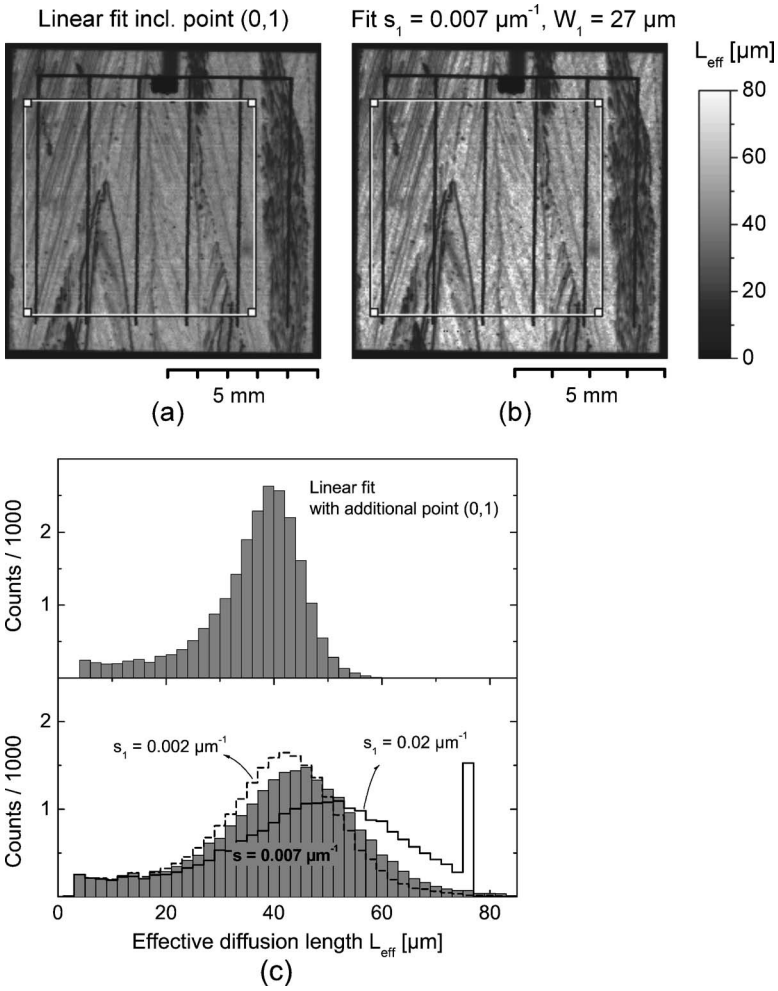

FIG. 5. (a) L_{eff} map obtained by linear fits to the values $\text{IQE}_i^{-1}(\alpha_i^{-1})$. The point (0,1) is included as additional data point. (b) L_{eff} map from the same data fitted with the exact function. (c) Histograms of the data shown in parts (a) and (b). Besides the presumed recombination velocity $s_1=0.007\ \mu\text{m}^{-1}$ (gray columns), histograms are shown for $s_1=0.002\ \mu\text{m}^{-1}$ (dashed line) and $s_1=0.02\ \mu\text{m}^{-1}$ (solid line). The data included in the histograms are taken from the areas of interest marked by frames in parts (a) and (b) only.

seed for epitaxial growth. This way, the film was thickened by 20–25 μm of APCVD Si with a doping concentration of 4×10^{16} cm^{-3}.

From the SOI films, small (1 cm^2) test thin-film solar cells with mesa structure were processed. The emitter was diffused from a $POCl_3$ source targeting a sheet resistivity of 80 $\Omega/\square$. While the emitter grid had a conventional structure, defined by photolithography, the base was contacted by evaporating an aluminum frame in a trench around the active cell area. After metallization, the samples were passivated in a remote hydrogen plasma, and finally a double layer antireflection coating was applied. Details on the process are given in Ref. 31.

B. Characterization methods

For electrical characterization the spectrally resolved light beam induced current (SR-LBIC) was mapped on the finished solar cells. The employed system uses laser sources of 750, 790, and 830 nm wavelength. Subsequently, their surfaces were mechanically polished, and they were treated 15–20 s with a Secco etch.[32] Etch pit density (EPD) maps were acquired using an automated microscope and specially developed image analysis algorithms. Details on this system are published elsewhere.[33]

Before correlating effective diffusion length with EPD data, several effects were taken into account.

Firstly, the linear relationship between IQE^{-1} and α^{-1} is valid in the case of bulk diffusion length much smaller than layer thickness only. This requirement is not satisfied in the investigated devices. Therefore, we fitted the data $\text{IQE}_i^{-1}(\alpha_i^{-1})$ at each measured point with the exact analytical function $\text{IQE}^{-1}(\alpha^{-1})$ which is obtained by inserting Eqs. (38) and (25) into Eq. (19), and then calculating Eq. (28). In Eq. (38), W has to be replaced by the thickness of the p-layer W_1, and s has to be replaced by the effective surface recombination velocity s_1 at the p-p+ junction. The value of s_1 was estimated from the change in doping concentration at the interface between the highly doped p+ seed film and the about 10^{16} cm^{-3} doped p epitaxial layer. For this purpose, we used the analytical expression given by Godlewski *et al.*,[34] additionally taking into account apparent band-gap narrowing (BGN). Effective carrier concentrations, BGN energy model, and coefficients for slope/onset were taken from Refs. 35–37, respectively. Doping dependence of mobilities was considered by the empirical Caughey and Thomas model,[38] using the coefficient suggested in the PC1D simulation software.[36]

For the investigated samples, the model yields $S_1=1500$ cm s^{-1}, corresponding to $s_1=S_1/D_1=0.007\ \mu\text{m}^{-1}$. Figure 5 visualizes the difference between a L_{eff} map that was obtained by fitting the data with the exact function and

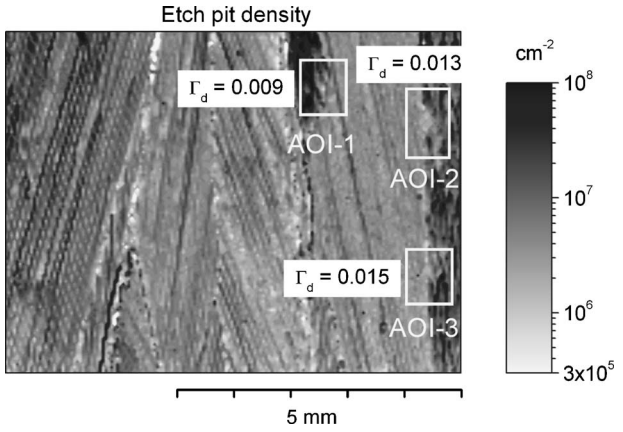

FIG. 6. EPD map of the sample for which L_{eff} data are shown in Fig. 5. In the marked areas of interest (AOI), L_{eff} and EPD data were correlated and fitted with the modified Donolato model (see Fig. 7).

one that was calculated by using the linear approximation. Additionally, in the histograms the effect of an error in s_1 on the distribution of L_{eff} values is examined.

Secondly, at LBIC measurements, effective diffusion length is not determined by material properties at the measurement point only, but is also affected by material quality in surrounding areas. One reason is the finite diameter of the laser beam and its intensity profile. The beam of the employed system has a full width at half maximum of approximately 50 μm, and its shape is assumed Gaussian. Another reason is carrier diffusion from the point of injection into neighboring areas and recombination at defects there. As a consequence, L_{eff} maps are always somewhat "blurred." To consider this effect in our calculation, we convolved the EPD data with a kernel function. This kernel is computed by convolution of a Gaussian function that represents the beam profile and a modified Bessel function of the second kind of order zero K_0 that represents carrier diffusion from an injection point source.[39] The decay constant L_l that enters into the modified Bessel function was set to the average measured diffusion length $\bar{L}_{\text{eff}}$ in the examined area of interest. The data resulting from convolution of EPD data and beam profile/diffusion kernel were named effective dislocation density (EDD).

Thirdly, the local correlation of single LBIC and EPD data points from two maps requires the very precise match of both coordinate systems. This was ensured by converting the LBIC data to the EPD coordinate system using translational and rotational transformations.

TABLE IV. Sensitivity of the fit parameters L_0 and Γ_d on the effective diffusion length L_l. The parameter L_l describes carrier diffusion from the point of generation and affects the convolution kernel used to transform the EPD map into an EDD map. Normally, L_l was set to the average effective diffusion length $\bar{L}_{\text{eff}}$ within the AOI (values marked with an asterisk).

Area of interest	L_l (μm)	L_0 (μm)	Γ_d
AOI-1	15	48	0.008
	30*	52	0.009
	50	57	0.010
AOI-2	20	54	0.012
	35*	63	0.013
	60	85	0.015
AOI-3	25	66	0.013
	40*	80	0.015
	60	111	0.016

C. Recombination strength results

Figure 6 shows a typical EPD map of an epitaxially thickened ZMR seed film together with normalized recombination strength values, determined by the model developed in the preceding sections. The corresponding L_{eff} map of the same sample is shown in Fig. 5(b). The specific fit function was determined by insertion of Eqs. (30), (38), and (36) into Eq. (32). Fit parameters were the normalized recombination strength Γ_d and the bulk diffusion length in the dislocation-free material L_0. As before, the effective back surface recombination velocity was estimated from doping data, yielding the above-mentioned value s_1=0.007 μm^{-1}. Best-fit curves for the three marked areas of interest (AOI) are plotted in Fig. 7, yielding recombination strength values Γ_d from 0.009 to 0.015 and diffusion length values L_0 in the range of 52–80 μm.

In our algorithm, carrier diffusion from the point of generation into neighboring regions is taken into account by convolving the L_{eff} map with a filter kernel. The local decay constant L_l that is entered into the kernel function is not known *a priori*. Theoretically, the problem can only be solved iteratively, since the dependence of L_{eff} on the dislocation density has to be used as input. As described above, we approximated L_l by the average diffusion length within the examined AOI $\bar{L}_{\text{eff}}$. The effect of L_l on best-fit parameters was investigated by a sensitivity analysis (Table IV). The recombination strength Γ_d varies only slightly with L_l, and compared to other uncertainties, such as measurement errors, the effect is negligible. In particular, a dislocation line has a

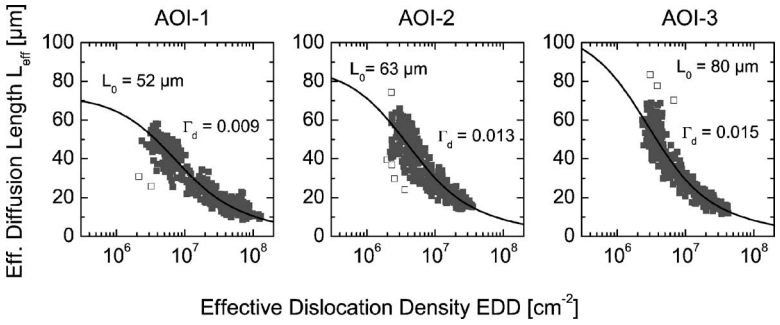

FIG. 7. Correlation of EPD and L_{eff} data (symbols) from the areas of interest marked in Fig. 6, and simulation with the modified version of Donolato's model (line). Data points drawn with open symbols were not considered in the fit.

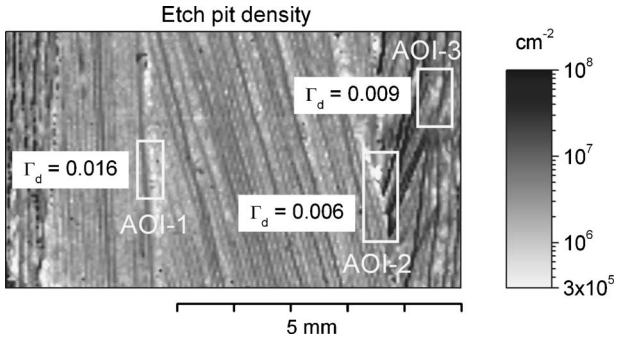

FIG. 8. EPD map from a sample produced with same technology as the one analyzed in Fig. 6. In the marked areas of interest (AOI), L_{eff} and EPD data were correlated and fitted with the modified Donolato model.

low dimension, compared to surface and volume recombination entities. Therefore, major changes in Γ_d are necessary to produce a significant change in the overall recombination activity. The effect of L_l on L_0 is more pronounced, but due to the lack of data points near $\rho_d=0$ (Fig. 7), the accuracy of the fit value for L_0 is limited anyway.

The EPD map shown in Fig. 8 was measured on a sample produced with the same technology as the one analyzed in Fig. 6. Ranging from 0.006 to 0.016, recombination strength values Γ_d are of similar magnitude as those in the former sample. The corresponding best fit values for L_0 in the areas labeled "AOI-1," "AOI-2," and "AOI-3" are 177, 67, and 76 μm, respectively.

D. Discussion on experimental data

In both thin-film solar cells presented above, similar recombination strength values were measured. The fairly regular distribution of defects resulting from the ZMR process supports this finding. However, we have to be aware that the minimum area yielding a single recombination strength value with sufficient accuracy is approximately 1 mm^2 (corresponding to ~400 data points). The method is therefore not suitable to study microscopic effects, such as enhanced recombination activity at single dislocation clusters.

Remarkably, in both EPD maps (Figs. 6 and 8) the lowest Γ_d values are found in AOIs with the highest "contrast", i.e., regions including points with very low as well as very high dislocation density. However, it has to be taken into account that with increasing dislocation density the amount of clustered, overlapping etch pits increases and therefore measurement accuracy decreases.

Our experimental values fit well to the data found in literature (Table V). Extensive work has been published by a group at TU Bergakademie Freiberg.[6,8,10] Largely, the experimental methods used by Lawerenz *et al.* and Rinio *et al.* are similar to those presented here. For diffusion length measurement on unprocessed wafers, they used the surface photovoltage (SPV) method, while for finished solar cells they employed the LBIC technique. Etch pit counting was also done by optical microscopy and automated image analysis. However, differences exist concerning data processing: (i) dislocations near the point of carrier injection were considered in a partly different way,[8] and (ii) LBIC quantum efficiency data were taken for a single wavelength only. Effective diffusion length was then calculated through a numerical model for the specific solar cell type, while in our calculation only analytical expressions are involved. However, the recombination strength values we determined for thin-film solar cells are similar to the ones measured for conventional multicrystalline Si solar cells. This holds even though for the investigated thin-film Si samples, dislocation density was much higher (1×10^6–5×10^7 cm^{-2}) than for typical multicrystalline Si solar cells (1×10^4–5×10^6 cm^{-2}).

TABLE V. Recombination strength data found in literature.

Sample type (all based on mc-Si)	Lifetime meas. method	Typical Γ_d (extreme Γ_d)	Remarks	Reference
Unprocessed wafers	SPV	0.01–0.04		6
Solar cells	LBIC	0.001–0.008		6
Solar cells	LBIC	0.001–0.006 (<0.0003–0.016)	Different diffusion processes (tube furnace and RTP)	8
Solar cells	LBIC	<0.001–0.008	Values are reduced to ~20% after hydrogen passivation	9
Solar cells	LBIC	0.003–0.006	Values are reduced to ~20% after hydrogen passivation	10
Heterojunction solar cells	LBIC	0.0001–0.005	Low temp. *a*-Si emitter	10
SiN_x passivated wafers	CDI	0.0006–0.003		11
Not published	Not published	0.2	Fit of data by Imaizumi *et al.*[a]	4

[a]Reference. 3.

The results found here are also in line with earlier results by the authors investigating recombination strength using infrared lifetime mapping/carrier density imaging (ILM/CDI) for effective lifetime measurements.[11]

The only incompatible data in Table V are the one from Ref. 4. The recombination strength given in this work is one to two orders of magnitude higher than the other values. Donolato obtained these results by applying his model to the data published in Ref. 3. However, in the original publication neither the techniques for dislocation density and carrier lifetime measurement are mentioned nor is a statement made regarding whether the values were measured on raw wafers or on finished solar cells.

IV. CONCLUSIONS

The concept of an effective diffusion length can be used to describe recombination at different sites in a semiconductor specimen (bulk, surface, etc.) by a single parameter. It is also useful to describe inhomogeneous materials, such as multicrystalline Si wafers containing dislocations and grain boundaries. In a short review different definitions of an "effective diffusion length" have been summarized, and interconnections and differences have been worked out.

For the effect of dislocations on effective diffusion length, Donolato has presented an analytical model. However, as pointed out in this work, the definition of "effective diffusion length" he introduced in the original work is not useful concerning (i) compatibility with common measurement methods and (ii) representation of the actual operational state of a solar cell. Donolato's model therefore has been modified to be compatible with the "quantum efficiency effective diffusion length." It has been shown that for a semi-infinite specimen it is not of importance whether Donolato's or the quantum efficiency definition of effective diffusion length is used. However, for specimen of finite thickness both definitions yield very different results.

Donolato's model has been extended for the application to thin specimens with a finite recombination velocity at the rear side. Since the associated boundary value problem does not allow a straightforward analytical solution, we derived an approximate expression and validated the method by numerical computations using typical data.

Our model has been applied to the analysis of thin-film crystalline Si solar cells fabricated by ZMR and CVD technology. Maps of effective diffusion length and etch pit density have been measured by SR-LBIC and by image analysis, respectively. From these data, recombination strength values Γ_d in the range of 0.006–0.016 have been determined. These fit very well to results measured on conventional multicrystalline Si solar cells.

ACKNOWLEDGMENTS

The authors would like to thank the technical staff from the Fraunhofer ISE Solar Cell Department for preparing thin-film solar cells and carrying out diffusion length measurements. One of the authors (T.K.) has been supported by the scholarship program of the German Federal Environmental Foundation. This work was supported in part by the state of Baden-Württemberg in the framework of the FAKT project.

[1] H. El Ghitani and S. Martinuzzi, J. Appl. Phys. **66**, 1717 (1989).
[2] C. van Opdorp, A. T. Vink, and C. Werkhoven, in *Proceedings of the Sixth International Symposium on Gallium Arsenide and Related Compounds, St. Louis, MO, 1976*, edited by L. F. Eastman [Inst. Phys. Conf. Ser. **33**, 317 (1977)].
[3] M. Imaizumi, I. Tadashi, M. Yamaguchi, and K. Kaneko, J. Appl. Phys. **81**, 7635 (1997).
[4] C. Donolato, J. Appl. Phys. **84**, 2656 (1998).
[5] C. Donolato, *Proceedings of the Fifth International Workshop on Beam Injection Assessment of Defects in Semiconductors (BIADS 98), Schloss Wulkow, Germany, 1998* [Solid State Phenom. **63–64**, 45 (1998)].
[6] A. Lawerenz, M. Rinio, S. Riedel, M. Ghosh, M. Werner, and H. J. Möller, in *Proceedings of the 16th European Photovoltaic Solar Energy Conference, Glasgow, UK, 2000*, edited by H. Scheer, B. McNelis, W. Palz, H. A. Ossenbrink, E. Dunlop, and P. Helm (James and James Ltd., London, UK, 2000), pp. 1647–1650.
[7] S. Riedel, M. Rinio, and H. J. Möller, in *Proceedings of the 17th European Photovoltaic Solar Energy Conference, Munich, 2001*, edited by W. Palz, B. McNelis, H. A. Ossenbrink, and P. Helm (WIP Renewable Energies, Munich, 2001), pp. 1412–1415.
[8] M. Rinio, S. Peters, M. Werner, A. Lawerenz, and H. J. Möller, in *Proceedings of the Ninth International Autumn Meeting on Gettering and Defect Engineering in Semiconductor Technology (GADEST 2001) Catania, Italy, 2001* [Solid State Phenom. **82–84**, 701 (2002)].
[9] M. Rinio, A. Hauser, and H. J. Möller, in *Proceedings of the Third World Conference on Photovoltaic Energy Conversion, Osaka, Japan, 2003*, edited by L. L. Kazmerski, K. Kurokawa, B. McNelis, M. Yamaguchi, C. Wronski, and W. C. Sinke (WCPEC-3 Organizing Committee, Osaka, Japan, 2003), Vol. A, pp. 118–121.
[10] M. Rinio, E. Zippel, and D. Borchert, in *Proceedings of the 20th European Photovoltaic Solar Energy Conference and Exhibition, Barcelona, Spain, 2005*, edited by W. Palz, H. Ossenbrink, and P. Helm (WIP Renewable Energies, Munich, 2005), pp. 706–709.
[11] S. Riepe, G. Stokkan, T. Kieliba, and W. Warta, in *Proceedings of the Tenth International Autumn Meeting on Gettering and Defect Engineering in Semiconductor Technology (GADEST), Zeuthen, Germany, 2003*, edited by H. Richter and M. Kittler [Solid State Phenom. **95–96**, 229 (2004)].
[12] C. Donolato, Appl. Phys. Lett. **46**, 270 (1985).
[13] T. Markvart, IEEE Trans. Electron Devices **43**, 1034 (1996).
[14] K. Misiakos and F. A. Lindholm, J. Appl. Phys. **58**, 4743 (1985).
[15] C. Donolato, J. Appl. Phys. **66**, 4524 (1989).
[16] M. A. Green, J. Appl. Phys. **81**, 268 (1997).
[17] U. Rau and R. Brendel, J. Appl. Phys. **81**, 6412 (1998).
[18] C. Donolato, Semicond. Sci. Technol. **7**, 37 (1992).
[19] M. Abramowitz and I. A. Stegun, *Handbook of Mathematical Functions* (Dover, New York, 1972).
[20] R. Brendel, *Thin-Film Crystalline Silicon Solar Cells: Physics and Technology* (Wiley-VCH, Weinheim, 2003), p. 55.
[21] P. A. Basore, *Proceedings of the 23rd IEEE Photovoltaic Specialists Conference, Louisville, KY, 1993* (IEEE, New York, 1993), pp. 147–152.
[22] N. D. Arora, S. G. Chamberlain, and D. J. Roulston, Appl. Phys. Lett. **37**, 325 (1980).
[23] J. Dugas and J. Qualid, Sol. Cells **20**, 167 (1987).
[24] M. Spiegel, B. Fischer, S. Keller, and E. Bucher, *Proceedings of the 28th IEEE Photovoltaic Specialists Conference, Anchorage, AK, 2000* (IEEE, New York, 2000), pp. 311–314.
[25] J. Isenberg, O. Bartels, and W. Warta, *Proceedings of the 29th IEEE Photovoltaic Specialists Conference, New Orleans, LA, 2002* (IEEE, New York, 2002), pp. 328–331.
[26] S. M. Sze, *Physics of Semiconductor Devices*, 2nd ed. (Wiley, New York, 1981), p. 87.
[27] C. Donolato, *Proceedings of the Fifth International Conference on Polycrystalline Semiconductors (POLYSE '98), Schwäbisch Gmünd, Germany, 1998* [Solid State Phenom. **67–68**, 75 (1999)].
[28] R. Brendel, *Thin-Film Crystalline Silicon Solar Cells: Physics and Technology* (Wiley-VCH, Weinheim, 2003), p. 56.
[29] R. Brendel and U. Rau, J. Appl. Phys. **85**, 3634 (1999).
[30] R. A. Sinton, in *Proceedings of the Third World Conference on Photovoltaic Energy Conversion, Osaka, Japan, 2003*, edited by L. L. Kazmerski, K. Kurokawa, B. McNelis, M. Yamaguchi, C. Wronski, and W. C. Sinke (WCPEC-3 Organizing Committee, Osaka, Japan, 2003), pp. 1028–1031.

[31]S. Reber, W. Zimmermann, and T. Kieliba, Sol. Energy Mater. Sol. Cells **65**, 409 (2001).
[32]F. Secco D'Aragona, J. Electrochem. Soc. **119**, 948 (1972).
[33]T. Kieliba, Ph.D. thesis, Universität Konstanz, 2006.
[34]M. P. Godlewski, C. R. Baraona, and H. W. Brandhorst, Sol. Cells **29**, 131 (1990).
[35]S. M. Sze, *Physics of Semiconductor Devices*, 2nd ed. (Wiley, New York, 1981), p. 143.
[36]D. A. Clugston and P. A. Basore, *Proceedings of the 26th IEEE Photovoltaic Specialists Conference, Anaheim, CA, 1997* (IEEE, New York, 1997), pp. 207–210.
[37]A. Cuevas, M. Stuckings, J. Lau, and M. Petravic, in *Proceedings of the 14th European Photovoltaic Solar Energy Conference, Barcelona, Spain, 1997*, edited by H. A. Ossenbrink, P. Helm, and H. Ehmann (H. S. Stephens & Associates, Bedford, UK, 1997), pp. 2416–2419.
[38]D. M. Caughey and R. E. Thomas, Proc. IEEE **55**, 2192 (1967).
[39]R. Brendel, M. Bail, B. Bodmann, J. Kentsch, and M. Schulz, Appl. Phys. Lett. **80**, 437 (2002).